ELSEVIER

Propagation of acoustic waves in a visco-elastic two-phase system: influences of the liquid viscosity and the internal diffusion

M. Ichihara[a,*], M. Kameda[b]

[a] Earthquake Research Institute, University of Tokyo, Yayoi, Bunkyo, Tokyo 113-0032, Japan
[b] Department of Mechanical Systems Engineering, Tokyo Noko University, Koganei, Tokyo 184-8588, Japan

Abstract

The main purpose of the present paper is to present the mathematical expression for the frequency-dependent effective acoustic properties of a liquid–bubble mixture. Effects of the bubble resonance, the heat and mass transfer between the liquid and bubbles, and the viscoelasticity of the liquid are included in the expression. Several characteristic frequencies associated with these internal processes are represented by simple functions of the material and condition parameters. Using these expressions, the acoustic properties of bubbly magmas are calculated and analyzed. It is shown that the dispersion and attenuation of the pressure wave are particularly considerable in the frequency range lower than the characteristic frequency of the mass transfer and in the range near the characteristic frequency of the viscous response of the bubble radius. In the frequency range bounded by these two frequencies, the bubbly magma can be regarded as an elastic medium with the slow sound speed. The significance of such acoustic properties on resonance of a body of bubbly magma is demonstrated in a simple one-dimensional system.
© 2004 Elsevier B.V. All rights reserved.

Keywords: pressure wave; bubble; wave dispersion; attenuation; gas diffusion; resonance

1. Introduction

It is generally considered that the sound speed of magma is significantly reduced by the presence of bubbles. Many features of seismo-acoustic activities of volcanoes are ascribed to the reduced sound speed of the magma (e.g., Chouet, 1996; Benoit and McNutt, 1997; Kumagai and Chouet, 2000; Garces and McNutt, 1997; Neuberg et al., 2000). However,

other essential aspects of the acoustic properties of liquid–bubble mixtures are the dispersion and attenuation, which have not been considered sufficiently in previous studies on the volcanic phenomena. This paper focuses on the dispersion and attenuation of the pressure waves in the bubbly magma.

As the pressure wave propagates in the bubbly magma, the liquid and bubbles cease to be in equilibrium, and internal processes are set up toward restoration of equilibrium. The bubbles tend to expand or shrink so as to restore the mechanical equilibrium. In addition, the expansion or compression of the bubbles perturbs the thermodynamic equilibrium so that the heat and the volatile components are transferred between the liquid and bubbles. These process-

* Corresponding author. Tel.: +81-3-5841-5776; fax: +81-3-3812-9417.

E-mail addresses: ichihara@eri.u-tokyo.ac.jp (M. Ichihara), kame@cc.tuat.ac.jp (M. Kameda).

es control the volume change of the bubbles and, eventually, the apparent compressibility of the mixture. However, the restoration of the equilibrium does not always follow the pressure change in the wave field. Immediate expansion or compression of the gas in the bubbles is prevented by viscous resistance and inertia of the liquid. The heat and mass transfer by diffusion takes place comparatively slowly. The delay of the internal processes causes the rate-dependent response of the mixture and attenuation of the pressure wave.

There exists a number of literatures on the acoustic properties of a bubbly liquid with viscosity as low as that of water. The characteristics of the wave dispersion and attenuation have been investigated theoretically (Commander and Prosperetti, 1989; Varadan et al., 1985; Gaunaurd and Überall, 1981; Prosperetti, 1984; Caflish et al., 1985) and experimentally (Cheyne et al., 1995; Silberman, 1957). Good agreement has been obtained between the theoretical and experimental results. In the low viscosity liquids, the dispersion and attenuation of the waves are mainly caused by the resonant scattering of bubbles (Commander and Prosperetti, 1989; Gaunaurd and Überall, 1981) and the heat transfer between the liquid and bubbles (Prosperetti, 1991).

On the other hand, understandings of the acoustic properties of bubbly magmas are not sufficient. In volcanic systems, the magma viscosity is an important controlling parameter. Lensky et al. (2002) recently demonstrated a possibility that the effective bulk viscosity of the bubbly magma has a negative value due to the non-linear coupling between the viscous resistance against the bubble expansion and the volatile diffusion from the liquid to the bubble. They derived a notable conclusion that this negative bulk viscosity can cause amplification of seismic waves. However, because of the non-linear nature of the process, their conclusion may not be applicable to the general cases.

The main purpose of the present paper is to present the mathematical expressions for the effective acoustic properties of a liquid–bubble mixture. Effects of the viscoelasticity of the liquid, the volatile diffusion, the bubble resonance and the heat transfer are included in the expressions. They are useful in evaluating the speed and attenuation of the pressure wave as a function of the frequency in various conditions. Char-

acteristics of the frequency dependence of the wave speed and attenuation changes at the time scales of the internal processes such as the viscous resistance against the bubble expansion (contraction), the bubble resonance and the volatile diffusion. These time scales are expressed by simple functions of the parameters representing the material properties (viscosity, elastic moduli, heat and mass diffusivities, etc.) and the condition (pressure, temperature, void fraction, etc.). As an example of the applications, the resonance behavior of a layer of bubbly magma is investigated. It is shown that the resonance of the bubbly magma depends considerably on the dispersion and attenuation of the waves due to the internal processes.

2. Mathematical formulation

2.1. Bulk modulus of a bubble

The bulk modulus of a bubble, K_g, is defined as:

$$K_g = -\frac{R}{3}\frac{\partial P_g}{\partial R},\tag{1}$$

where P_g is the pressure in the bubble and R is the bubble radius.

The bubble should also be regarded as a viscoelastic body with the bulk modulus depending on the frequency. For example, the bulk modulus of an ideal-gas bubble in an adiabatic process ($P_g R^{3\gamma} =$ constant) is $K_g = \gamma P_g$, where γ is the specific heat ratio. If the oscillation is very slow, the process is more likely to be isothermal ($P_g R^3 =$ constant) so that $K_g = P_g$. Taking account of thermal diffusion in the bubble, Prosperetti (1991) formulated the bulk modulus of a bubble in a periodic pressure field ($\propto e^{-i\omega t}$) as:

$$\frac{K_g}{P_o} = \frac{\gamma\Theta^2}{\Theta[\Theta + 3(\gamma-1)A_-] + 3i(\gamma-1)(\Theta A_+ - 2)},\tag{2}$$

$$A_{\pm} = \frac{\sinh\Theta \pm \sin\Theta}{\cosh\Theta - \cos\Theta},$$

$$\Theta = R\sqrt{\frac{2\omega}{\kappa_T}},\tag{3}$$

where P_o is the static pressure, that is the center of the oscillation of P_g, and κ_T is the thermal diffusivity of the gas in the bubble.

The volumetric change of a bubble is influenced also by the volatile transfer between the liquid and bubble. The process is controlled by the diffusion of the volatile in the liquid. Including this effect, we have formulated the effective bulk modulus of a bubble as:

$$\frac{K_g}{P_o} = \gamma\Theta^2 / \{\Theta[\Theta + 3(\gamma-1)A_- + 3\gamma A_g\sqrt{\alpha_g}]$$
$$+ 3i[(\gamma-1)(\Theta A_+ - 2) + \gamma A_g(\sqrt{\alpha_g}\Theta + 2\alpha_g)]\}, \tag{4}$$

$$A_g = \frac{\rho_l P_o}{\rho_g}\frac{\partial C_{eq}}{\partial P}, \tag{5}$$

$$\alpha_g = \frac{\kappa_{gl}}{\kappa_T}, \tag{6}$$

where ρ_l and ρ_g are the densities of the liquid and the gas, respectively, $C_{eq}(P)$ denotes the volatile concentration which is in equilibrium with the gas phase at pressure P, and κ_{gl} is the diffusivity of the volatile in the liquid. The physical meaning of the dimensionless parameter, A_g, is explained as follows. If the pressure change of ΔP is given in a quasi-static process, the mass of the volatile component in a unit volume of the liquid phase is to change by $\rho_l \Delta P \partial C_{eq}/\partial P$, while the gas density in the bubble is to change by $\rho_g \Delta P/P_o$. The ratio of the former to the latter is the parameter, A_g. The derivation process of Eq. (4) is explained in Appendix A.

2.2. Viscoelasticity of the liquid

For the present study, we employ the simplest linear viscoelastic model, which is quite general and often used to describe the fundamental features of elastic and viscous behaviors of silicate melts (Webb and Dingwell, 1995; Webb, 1997).

If a sinusoidal oscillation is applied to the viscoelastic material, the shear and bulk moduli are described by complex functions of the frequency of the oscillation (Webb and Dingwell, 1995;

Webb, 1997), which are denoted by μ_ω and K_ω, respectively:

$$\mu_\omega = \mu_\infty \frac{-i\omega\tau_s}{1 - i\omega\tau_s}, \tag{7}$$

$$K_\omega = K_o + (K_\infty - K_o)\frac{-i\omega\tau_v}{1 - i\omega\tau_v}, \tag{8}$$

where μ_∞ and K_∞ are the unrelaxed rigidity (shear modulus) and bulk modulus (volumetric modulus), respectively, and K_o is the equilibrium bulk modulus (relaxed modulus). The shear and volume relaxation times (τ_s and τ_v, respectively) are given as the ratio of the low frequency shear and bulk viscosity (η_o and ζ_o, respectively) and the relaxational part of the elasticity (Webb and Dingwell, 1995; Webb, 1997):

$$\tau_s = \eta_o/\mu_\infty, \tag{9}$$

$$\tau_v = \zeta_o/(K_\infty - K_o). \tag{10}$$

As the viscosity is a function of stress and strain rate, the complex shear and bulk moduli are converted into the complex viscosities, which are denoted by η_ω and ζ_ω, respectively:

$$\eta_\omega = \mu_\omega/(-i\omega), \tag{11}$$

$$\zeta_\omega = (K_\omega - K_o)/(-i\omega). \tag{12}$$

2.3. Effective properties of a liquid–bubble mixture

It is assumed that the acoustic property of a liquid–bubble mixture is represented by the effective bulk modulus (K_m), shear modulus (μ_m), and density (ρ_m), in the same way as a homogeneous material. The mathematical procedure to calculate these effective properties is described in the separate paper

(Ichihara et al., 2004). Here, we just present the final expressions:

$$K_m = \frac{K_\omega + \frac{4}{3}\phi\Gamma\mu_\omega}{1 - \phi\Gamma},$$

$$\Gamma = \frac{K_g - K_\omega}{K_g + \frac{4}{3}\mu_\omega}$$

$$\times \frac{1}{1 - \frac{\rho_1\omega^2 R^2}{3K_g + 4\mu_\omega}\left(1 + i\omega R\sqrt{\frac{\rho_1}{K_\omega + \frac{4}{3}\mu_\omega}}\right)}, \quad (13)$$

$$\mu_m = \mu_\omega\left[1 - \frac{\phi\left(1 - \frac{\mu_g}{\mu_\omega}\right)}{1 - \frac{2}{15}(1 - \phi)\left(3 + \frac{2\mu_\omega}{K_\omega + \frac{4}{3}\mu_\omega}\right)\left(1 - \frac{\mu_g}{\mu_\omega}\right)}\right], \quad (14)$$

$$\rho_m = \rho_g\phi + \rho_1(1 - \phi) \quad (|\mu_\omega| \sim |K_\omega|), \quad (15)$$

$$\rho_m = \rho_1\frac{1 - \phi(\rho_1 - \rho_g)/(\rho_1 + 2\rho_g)}{1 + 2\phi(\rho_1 - \rho_g)/(\rho_1 + 2\rho_g)}$$
$$(|\mu_\omega| \ll |K_\omega|), \quad (16)$$

where ϕ is the void fraction and μ_g is the shear modulus of the bubble which represents its deformability.

The expression of Eq. (13) represents a dynamical response of the mixture, which contains the bubble resonance with a resonance frequency obtained by the vanishing of the real part of the denominator of γ, and with the imaginary term in the denominator determining the radiation width of this resonance (Gaunaurd and Überall, 1981). With the relaxed ($\mu_\omega = 0$) and unrelaxed ($\mu_\omega = \mu_\infty$) shear moduli, the relaxed and unrelaxed resonance frequencies (denoted as ω_o and ω_∞, respectively) are determined as:

$$\omega_o = \frac{1}{R}\sqrt{\frac{3K_g}{\rho_1}} \quad (\omega_o\tau_s \ll 1), \quad (17)$$

$$\omega_\infty = \frac{1}{R}\sqrt{\frac{3K_g + 4\mu_\infty}{\rho_1}} \quad (\omega_\infty\tau_s \gg 1). \quad (18)$$

In case that the frequency is much smaller than the resonance frequency, Eq. (13) is simplified as:

$$K_m \sim \frac{K_\omega\left(K_g + \frac{4}{3}\mu_\omega\right) + \frac{4}{3}\phi\mu_\omega(K_g - K_\omega)}{\phi K_\omega + K_g + \frac{4}{3}\mu_\omega}. \quad (19)$$

Constitutive Eqs.(7) and (8) are substituted into Eq. (19), and $K_\infty - K_o = 0$ is assumed for simplicity. Assuming $\mu_\infty \gg \phi K_o + K_g$ (see Section 3.2 for the magma properties), Eq. (19) is approximated as:

$$K_m = \frac{K_o K_g}{\phi K_o + (1 - \phi)K_g}$$
$$+ \frac{\frac{4}{3}\mu_\infty\phi(1 - \phi)(K_o - K_g)^2}{\left[\phi K_o + (1 - \phi)K_g\right]\left[\phi K_o + (1 - \phi)K_g + \frac{4}{3}\mu_\infty\right]}$$
$$\times \frac{-i\omega\tau_m}{1 - i\omega\tau_m} \sim \frac{K_o K_g}{\phi K_o + (1 - \phi)K_g}$$
$$+ \frac{\phi(1 - \phi)(K_o - K_g)^2}{\phi K_o + (1 - \phi)K_g}\frac{-i\omega\tau_m}{1 - i\omega\tau_m}, \quad (20)$$

$$\tau_m = \frac{\left[\phi K_o + (1 - \phi)K_g + \frac{4}{3}\mu_\infty\right]\tau_s}{\phi K_o + (1 - \phi)K_g}$$
$$\sim \frac{4}{3}\frac{\eta_o}{\phi K_o + (1 - \phi)K_g} \quad (21)$$

where η_o is introduced according to Eq. (9). Eq. (20) has the same form as (8) with τ_m corresponding to the relaxation time. When $\omega\tau_m \gg 1$, we obtain $K_m \sim K_o$.

While for $\omega\tau_m \ll 1$, we obtain:

$$K_m \sim K_{mo} = \left(\frac{\phi}{K_g} + \frac{1-\phi}{K_o} \right)^{-1}, \tag{22}$$

where K_{mo} is the generally used bulk modulus of the liquid–bubble mixture (e.g., Garces, 1997).

The effective density is different between the cases that the matrix is close to a solid and to a fluid where relative motion between the inclusions and the matrix can occur. The effective density for a fluid matrix, Eq. (16), is governed by the inertia, while that for a solid matrix, Eq. (15), is governed by the gravity (Kuster and Toksöz, 1974).

The effective bulk and shear viscosities are calculated by $\zeta_m = (K_m - K_{mo})/(-i\omega)$ and $\eta_m = \mu_m/(-i\omega)$, respectively, in the same way as η_ω and ζ_ω. If it is assumed that the matrix is a Newtonian liquid ($K_\omega = K_o - i\omega\zeta_o$, $\mu_\omega = -i\omega\eta_o$) and the bulk modulus of the bubble is constant, the bulk viscosity of the mixture in the low-frequency limit is:

$$\lim_{\omega\to 0} \zeta_m = \frac{1-\phi}{[\phi + (1-\phi)K_g/K_o]^2}$$
$$\times \left[\frac{4}{3}\eta_o\phi\left(1 - \frac{K_g}{K_o}\right)^2 + \zeta_o\left(\frac{K_g}{K_o}\right)^2 \right],$$
$$\sim \frac{1-\phi}{(\phi + K_g/K_o)^2}\left[\frac{4}{3}\eta_o\phi + \zeta_o\left(\frac{K_g}{K_o}\right)^2 \right], \tag{23}$$

where we assume $K_g \ll K_o$ and $\phi \ll 1$. If we further assume $\phi \gg K_g/K_o$, we obtain:

$$\zeta_m \sim \frac{4}{3}\eta_o \frac{1-\phi}{\phi}. \tag{24}$$

Eq. (24) is often used to represent the bulk viscosity of a liquid–bubble mixture (e.g. Massol and Jaupart, 1999). On the other hand, the effective zero shear-rate viscosity is approximately:

$$\lim_{\omega\to 0} \eta_m = \eta_o \left(1 - \frac{5}{3} \frac{1 - \dfrac{\mu_g}{\mu_\omega}}{1 + \dfrac{2\mu_g}{3\mu_\omega}} \phi \right). \tag{25}$$

The parameter μ_g/μ_ω represents the deformability of the bubbles. Eq. (25) agrees with the Mackenzie's

expression: $\eta_m = \eta_o(1 - 5\phi/3)$ (Mackenzie, 1950; Llewellin et al., 2002) with completely deformable bubbles ($\mu_g/\mu_\omega = 0$), while it approaches the Sibree's expression: $\eta_m = \eta_o(1-\phi)^{-5/2}$ (Sibree, 1934; Massol and Jaupart, 1999) for $\phi \to 0$ with completely non-deformable bubbles ($\mu_g/\mu_\omega = \infty$). Several other models for the shear viscosity of liquid–bubble mixtures have been proposed. Most of the models suggest that the effective viscosity linearly increases with the increasing volume fraction of non-deformable bubbles and linearly decreases with the increasing fraction of deformable bubbles. Those models are reviewed and tested by Llewellin et al. (2002). Their experimental data were explained best by the Mackenzie's model for deformable bubbles and by the modified Taylor model ($\eta_m = \eta_o(1 + 9\phi)$) (Stein and Spera, 1992) for non-deformable bubbles. They also demonstrated that, as the frequency of the applied strain increases, the deformability of bubbles increases, and consequently the effective shear viscosity decreases. The transition of the deformability occurs at a frequency around:

$$\tau_{ca}^{-1} = S/(\eta_o R), \tag{26}$$

where S is the surface tension (Stein and Spera, 1992; Llewellin et al., 2002). We may represent such frequency dependence of the bubble deformability by defining:

$$\mu_g/\mu_\omega = 1/(\omega\tau_{ca})^2. \tag{27}$$

Actually, the contribution of μ_g to the effective shear modulus is of the order of ϕ and negligibly small in the present conditions ($\phi \ll 1$).

3. Physical parameters of the system

3.1. Physical parameters of the bubble

We assume that H_2O is the only volatile component in the liquid–bubble system. In order to calculate K_g and μ_g using Eqs. (4) and (27), we need the thermal diffusivity (κ_T), the specific heat ratio (γ), and P_o/ρ_g in the vapor phase, the diffusivity (κ_{gl}) and the solubility (C_{eq}) of H_2O in the melt, and the surface tension (S).

We evaluate the above parameters for the pressure up to 100 MPa, in which probability of existence of

bubbles in magma is large according to the content and the solubility of H_2O (Sparks et al., 1994; Holloway and Blank, 1994). The representative temperature of the system is regarded as 1000 °C (1273 K).

The surface tension for the H_2O vapor and silicate melt interface at 1000 °C is about 0.3 N/m at 0.1 MPa (Murase and McBirney, 1973) and decreases to 0.1 N/m at 100 MPa (Khitarov et al., 1979; Dingwell, 1998). Between these pressures, we assume that S is a linear function of log P.

Data in Table 1 (Bowers, 1995) show that the relation of H_2O gas density to the temperature and the pressure satisfies the equation of state for an ideal gas, Eq. (A2). Therefore, we regard the gas as an ideal gas. The heat capacity (C_p) of H_2O as an ideal gas with $\gamma = 1.3$ and $R_g = 462$ J/kg/K is 2000 J/kg/K, which is calculated by $C_p = R_g\gamma/(\gamma - 1)$. Although we see a factor of difference between this value and the measured heat capacity (Table 1), we use the former for consistency with the ideal-gas assumption. Actually, the difference is not significant in the following analyses and discussion which are concerned with the order of differences.

The heat conductivity is estimated by $\lambda_g = 0.1268T - 26.82$ mW/m/K, extrapolating the data measured below 1050 K (JSME, 1983). Its dependence on the pressure is negligible. At the temperature of 1273 K, we obtain $\lambda_g = 135$ mW/m/K. Using this value, the thermal diffusivity is calculated by Eq. (A6) (Table 1).

The diffusivity of H_2O in magma (κ_{gl}) depends on temperature, pressure, magma composition, and concentration and condition of H_2O (Zhang et al., 1991;
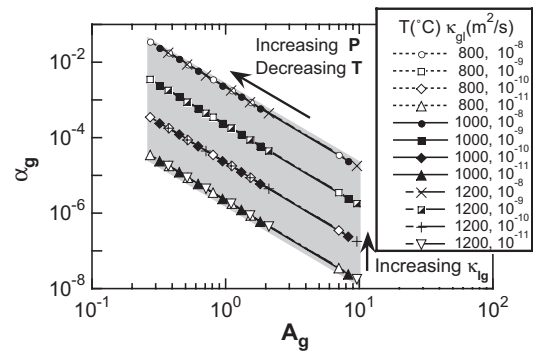

Fig. 1. The relevant range of the dimensionless parameters representing the effect of the volatile transfer in the magmatic systems is shown as the gray area. The parameter A_g and α_g are defined as Eqs. (5) and (6), respectively. The temperature (T) and the volatile diffusivity (κ_{gl}) are assumed as shown in the legend, and the pressure is varied from 0.1 to 100 MPa.

Zhang and Behrens, 2000; Nowak and Behrens, 1997; Proussevitch et al., 1993). In a rhyolitic melt at 1273 K, κ_{gl} is about 10^{-11} m²/s (Zhang et al., 1991; Zhang and Behrens, 2000; Nowak and Behrens, 1997). The diffusivity is larger by a few orders in a basaltic melt (Proussevitch et al., 1993). Therefore, we consider $10^{-11} < \kappa_{gl} < 10^{-8}$ m²/s and use $\kappa_{gl} = 10^{-9}$ m²/s as the standard value in the following analyses.

The solubility of H_2O calculated by Burnham model for various types of magma at 1273 K (Holloway and Blank, 1994) is reasonably fitted by:

$$C_{eq}(P) = (2.2 \pm 0.2) \times 10^{-6} P^{0.53}. \tag{28}$$

We use this relation with the coefficient of 2.2×10^{-6} in the following analyses.

The contributions of the material parameters to the bulk modulus of a bubble are collected in the two parameters, A_g and α_g, in Eqs. (4–6). Fig. 1 shows the possible range of these parameters in a magmatic system. The magma density (ρ_l) is assumed as 2600 kg/m³. The numerical values for A_g at $T = 1273$ K are listed in Table 1, too.

3.2. Physical parameters of magma

The magma properties are described by ρ_l, K_o, K_∞, μ_∞, τ_v, and τ_s. There exist a number of

Table 1
The material parameters and the dimensionless parameter A_g (Eq. (5)) for H_2O vapor at the temperature of 1273 K

P_o [MPa]	ρ_g [kg/m³]		C_p [J/kg/K]		κ_T [m²/s]	A_g
	Data	Ideal	Data	Ideal	Ideal	
0.1	0.170	0.170	2478	2000	3.97×10^{-4}	8.19
1.0	–	1.70	–		3.97×10^{-5}	2.78
2.5	4.26	4.25	2493		1.59×10^{-5}	1.80
5.0	8.53	8.51	2508		7.93×10^{-6}	1.30
10	17.1	17.0	2540		3.97×10^{-6}	0.940
25	43.0	42.5	2640		1.59×10^{-6}	0.611
50	87.0	85.1	2812		7.93×10^{-7}	0.441
100	175	170	3113		3.97×10^{-7}	0.319

The data are from Bowers (1995).

experimental studies on viscoelastic properties of silicate melts by using various techniques: ultrasonics (MHz frequencies), torsion deformation (mHz to Hz), fiber elongation (mHz), viscosity measurements (deformation rates of 10^{-3} s^{-1}), and so on. Useful compilations of the data can be found in Dingwell and Webb (1989), Webb and Dingwell (1995), and Webb (1997). Referring to these works we assume K_o, K_∞, and μ_∞ are constants represented by 20, 30 and 10 GPa, respectively. The relaxation time (or viscosity) of the shear deformation is treated as a variable parameter, assuming the equal relaxation times of the shear and volumetric deformation ($\tau_s = \tau_v$).

4. Results

4.1. Effects of heat and mass diffusion on the bulk modulus of a bubble

The effective bulk modulus of a bubble is calculated by Eq. (4) for some selected values of A_g and α_g. The thick broken lines in Fig. 2 are obtained from Eq. (2) without the effect of the volatile diffusion. As is noted in Section 2.1, the real parts of the broken line approaches the isothermal bulk modulus (P_o) and the adiabatic bulk modulus (γP_o) of the ideal gas in the low and high frequencies, respectively (Fig. 2a). The imaginary part, which represents the energy loss, has a peak around $\Theta^2 \sim 30$, where the transition between the isothermal and adiabatic conditions occurs. We define the inverse of the peak frequency as the characteristic time for the heat transfer (τ_T):

$$\tau_T = R^2 / (15\kappa_T). \tag{29}$$

The real part of K_g (Re K_g) including the volatile diffusion falls off in the low frequencies (Fig. 2a), where the imaginary part has another peak (Fig. 2b). The volatile transfer between the bubble and melt enhances the volumetric change of the bubble and increases the apparent compressibility (Re K_g^{-1}) and the loss of energy (Im K_g). The dimensionless peak frequency (denoted as Θ^2_{peak}) depends on both A_g and α_g in different ways. As α_g increases by an order, Θ^2_{peak} also increases by an order (compare the thick solid line and the lines with the solid marks in Fig. 2b). On the other hand, Θ^2_{peak} increases by two orders approximately (compare the thick solid line and the lines with the open marks), as A_g increases by an order.

We regard Θ^2_{peak} is important, because it represents the frequency below which the effect of volatile diffusion becomes significant. Its value is investigated over the relevant range of A_g and α_g, and plotted against $\alpha_g A_g^2$ (Fig. 3a). It has been found that values of Θ^2_{peak} fall on the broken line:

$$\Theta^2_{peak} = 18\alpha_g A_g^2, \tag{30}$$

even though there exist deviations from the line at the left end. When the data are re-plotted on the plane of $A_g^2 - \Theta^2_{peak}/\alpha_g$, all the points fall on a single curve (Fig. 3b).

Let us consider the physical meaning of the broken line relation (Eq. (30)). According to the
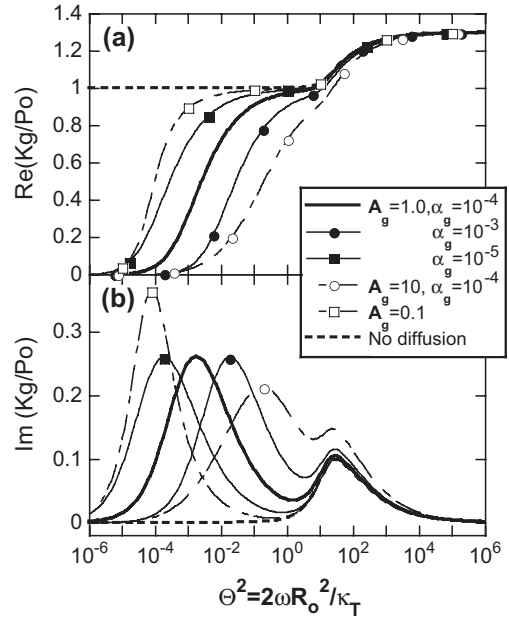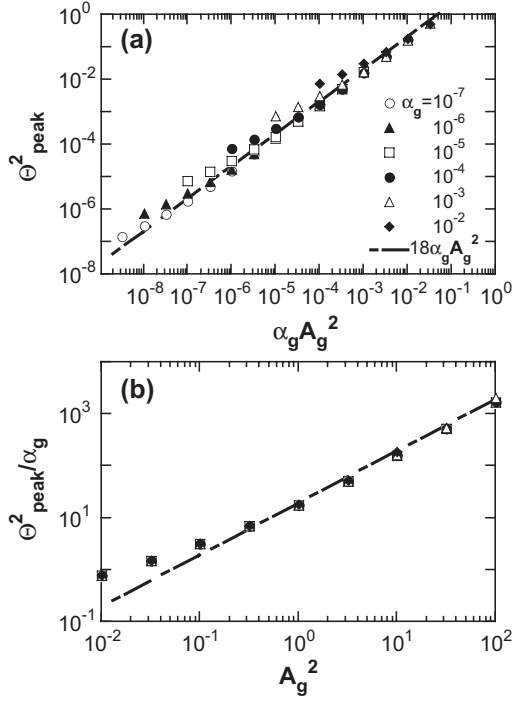

Fig. 2. The effective bulk modulus of a bubble calculated by Eq. (4) as a function of the dimensionless frequency. The real and the imaginary parts are presented in (a) and (b), respectively. The thick broken lines indicated as 'no diffusion' are obtained from Eq. (2), which eliminates the effect of the volatile diffusion.

Fig. 3. (a) Relation between the dimensionless frequency, Θ^2_{peak}, at which the imaginary part of the effective bulk modulus of a bubble takes the maximum value (Fig. 2b) and the dimensionless parameters, A_g and α_g. The relation is approximately represented by the broken line: $\Theta^2_{\text{peak}} = 18\alpha_g A_g^2$. (b) The same data are re-plotted on the plane of $\Theta^2_{\text{peak}}/\alpha_g$ versus A_g^2.

equation of state for an ideal gas, volume expansion of a bubble, δV_b, is:

$$\delta V_b = -\delta P \frac{m_{go} R_g T_o}{P_o^2} + \delta m_g \frac{R_g T_o}{P_o} = \delta V_P + \delta V_m,$$

$$(31)$$

where m_g is the total mass of the gas in the bubble, and the values at the center of oscillation are denoted with subscript 'o'. Here, δV_P represents the volumetric change due to the gas expansion, and δV_m represents the contribution of the mass transfer (δm_g). Significance of the latter contribution is evaluated by:

$$\frac{\delta V_m}{\delta V_P} = \frac{P_o}{m_{go}} \frac{|\delta m_g|}{|\delta P|}.$$

$$(32)$$

Because of mass conservation, δm_g should be compensated by the change of the volatile in the liquid, so that:

$$|\delta m_g| = \rho_l \left| \int_R^\infty 4\pi r^2 \delta C_g dr \right| = \rho_1 R^3 \delta P \frac{\partial C_{eq}}{\partial P}$$

$$\times \frac{4\pi \sqrt{\alpha_g}}{\Theta} \sqrt{1 + \frac{\sqrt{2\alpha_g}}{\Theta} + \frac{\alpha_g}{\Theta^2}},$$

$$(33)$$

where $\delta C_g = C_{go} C_*$ and C_* is given by Eqs. (A26) and (A28). The higher-order terms of α_g/Θ^2 is neglected when $\alpha_g/\Theta^2 \ll 1$. Substituting Eq. (33) and $m_{go} = (4\pi/3) R^3 \rho_g$ into Eq. (32), we obtain:

$$\frac{\delta V_m}{\delta V_P} \sim 3 \frac{\rho_1 P_o}{\rho_g} \frac{\partial C_{eq}}{\partial P} \frac{\sqrt{\alpha_g}}{\Theta} = \left(\frac{9\alpha_g A_g^2}{\Theta^2} \right)^{1/2}.$$

$$(34)$$

Eq. (34) indicates that the energy loss due to the mass transfer takes the maximum value when $\delta V_m = \delta V_P/\sqrt{2}$ according to Eq. (30). The contribution of the mass transfer is significant when $\delta V_m \gg \delta V_P$. The corresponding condition is $\Theta^2 \ll 9\alpha_g A_g^2 < \Theta^2_{\text{peak}}$. Actually, we can see the significant decrease of the bulk modulus of a bubble in such a range in Fig. 2a. We define the characteristic time of the effect of the volatile diffusion (τ_g) so that Eq. (30) is satisfied at $\omega = \tau_g^{-1}$:

$$\tau_g = \frac{R^2}{9\kappa_T \alpha_g A_g^2} = \frac{R^2}{9\kappa_{gl}} \left(\frac{\rho_1 P_o}{\rho_g} \frac{\partial C_{eq}}{\partial P} \right)^{-2}.$$

$$(35)$$

4.2. Effects of viscoelasticity of the liquid

The effective bulk and shear moduli of a liquid–bubble mixture are calculated by Eqs. (13) and (14), respectively. In order to focus on the effect of liquid viscoelasticity, we eliminate the effect of the heat and mass transfer by fixing the bulk modulus of a bubble (K_g) at 1 MPa in the analyses presented in this section. The void fraction and the bubble radius are assumed as $\phi = 0.03$ and $R = 10^{-3}$ m, respectively.

Two typical results are shown in Figs. 4 and 5, in which the real and the imaginary parts of K_m and μ_m are plotted against $\omega\tau_s$. For comparison, the values of
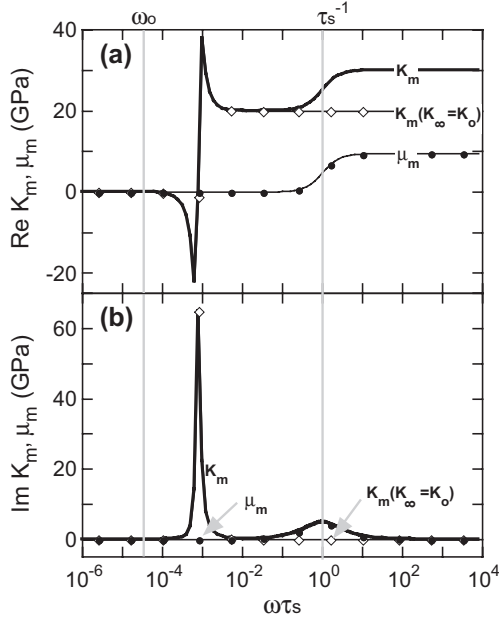
Fig. 4. The effective bulk modulus (K_m) and shear modulus (μ_m) of a liquid–bubble mixture calculated by Eqs. (13) and (14), respectively. The liquid viscosity (η_o) is assumed as 10 Pa s. The relaxed bulk modulus (K_o), the unrelaxed bulk modulus (K_∞), and the unrelaxed shear modulus (μ_∞) of the liquid are assumed as 20, 30 and 10 GPa, respectively. The bulk modulus of a bubble is fixed at 1 MPa independently of the frequency. For comparison, K_m for $K_\infty = K_o = 20$ GPa is shown (the thinner lines with diamonds). The relevant characteristic frequencies are shown with the gray lines, which are associate with the relaxation of the liquid (τ_s^{-1}) and the bubble resonance in the relaxed liquid (ω_o).

K_m with $K_\infty = K_o$ are shown by the lines with diamonds. The characteristic frequencies shown in the figures are those associated with the relaxation of the liquid (τ_s^{-1}: Eq. (9)), the volumetric relaxation of the mixture (τ_m^{-1}: Eq. (21)), and the bubble resonance in the relaxed and unrelaxed state of the liquid (ω_o and ω_∞: Eqs. (17) and (19)). Although we assumed $K_\infty - K_o = 0$ in obtaining Eq. (21) to calculate τ_m, its applicability to the present system is justified by the agreement of the thick lines and the thin lines with open diamonds around $\omega \sim \tau_m^{-1}$ (Fig. 5). It is noted that the bulk modulus is significantly decreased by the bubbles, but only in the low-frequency range. The range is bounded by ω_o in case that the viscosity is relatively low and the bubble resonance occurs in the relaxed state of the liquid (Fig. 4). In the higher-viscosity liquids, it is bounded by τ_m^{-1} (Fig. 5).

4.3. Dispersion and attenuation of pressure waves

The dispersion relation for pressure waves in the liquid–bubble mixture is given in the same way as in an elastic medium:

$$\frac{\omega^2}{k_m(\omega)^2} = \frac{K_m(\omega) + \frac{4}{3}\mu_m(\omega)}{\rho_m}, \tag{36}$$

$$c_m(\omega) = \frac{\omega}{\mathrm{Re}k_m(\omega)}, \tag{37}$$

$$Q_m^{-1}(\omega) = \frac{2\mathrm{Im}k_m(\omega)}{\mathrm{Re}k_m(\omega)}, \tag{38}$$

where k_m, c_m and Q_m^{-1} denote the wave number, the phase velocity and the attenuation factor of the
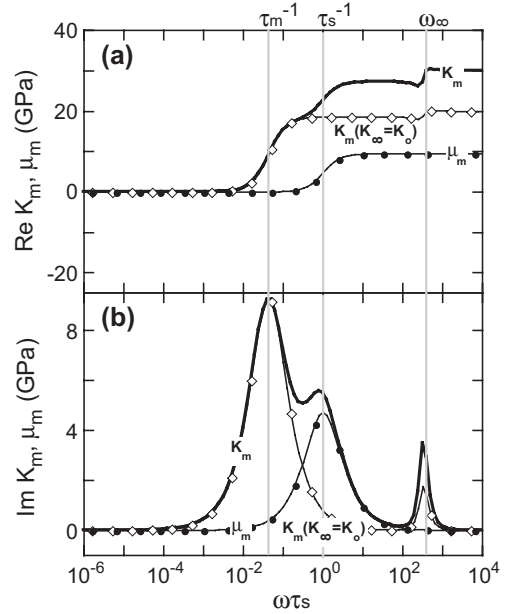

Fig. 5. The effective bulk modulus (K_m) and shear modulus (μ_m) of a liquid–bubble mixture calculated by Eqs. (13) and (14), respectively. The liquid viscosity (η_o) is assumed as 10^6 Pa s. Values of the moduli are assumed as $K_o = 20$ GPa, $K_\infty = 30$ GPa, and $\mu_\infty = 10$ GPa, and $K_g = 1$ MPa, in the same way as in Fig. 4. For comparison, K_m for $K_\infty = K_o = 20$ GPa is shown (the thinner lines with diamonds). The relevant characteristic frequencies are shown with the gray lines, which are associate with the relaxation of the liquid (τ_s^{-1}), the volumetric relaxation of the mixture (τ_m^{-1}), and the bubble resonance in the unrelaxed liquid (ω_∞).
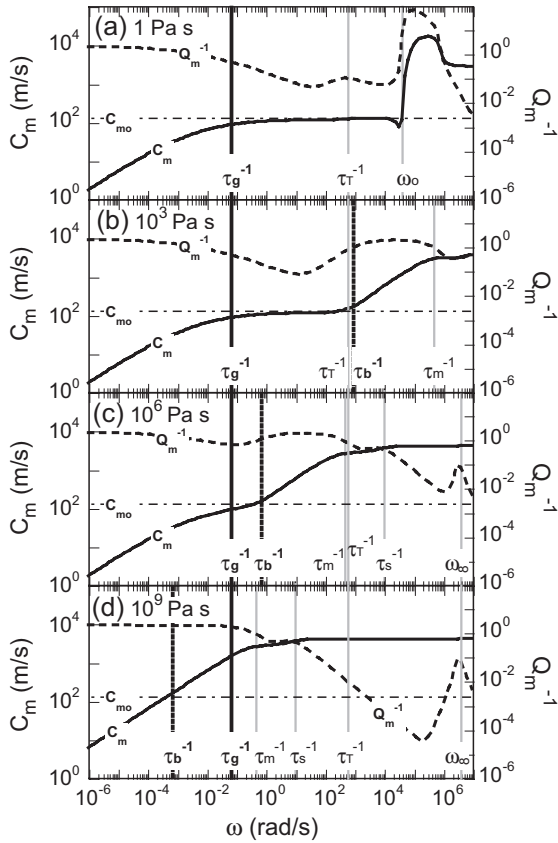
Fig. 6. The phase velocity (c_m) and the attenuation (Q_m^{-1}) of the pressure waves in the liquid–bubble mixture with various viscosities (η_o). The hydrostatic pressure (P_o) is assumed as 1 MPa. Values of the liquid moduli are assumed as $K_o = 20$ GPa, $K_\infty = 30$ GPa, and $\mu_\infty = 10$ GPa. The void fraction is $\phi = 0.03$. The parameters representing the properties of the vapor are given in Table 1. The diffusion coefficient of the volatile in the liquid (κ_{gl}) is assumed as 10^{-9} m^2/s. The characteristic frequencies of the acoustic properties of the mixture (Table 2) are indicated with the lines. The horizontal dash-and-dot line represents the value of c_{mo} defined by Eq. (39).

for the void fraction, and $R = 10^{-3}$ m for the bubble radius.

On the figures are indicated the characteristic frequencies for the heat transfer (τ_T^{-1}: Eq. (29)), the volatile diffusion (τ_g^{-1}: Eq. (35)), the stress relaxation of the liquid (τ_s^{-1}: Eq. (9)), the volumetric relaxation of the mixture (τ_m^{-1}: Eq. (21)), and the bubble resonance in the relaxed and unrelaxed conditions (ω_o and ω_∞: Eqs. (17) and (18)). The numerical values of these characteristic frequencies are listed in Table 2. These various internal processes bring about the complex dependence of the phase
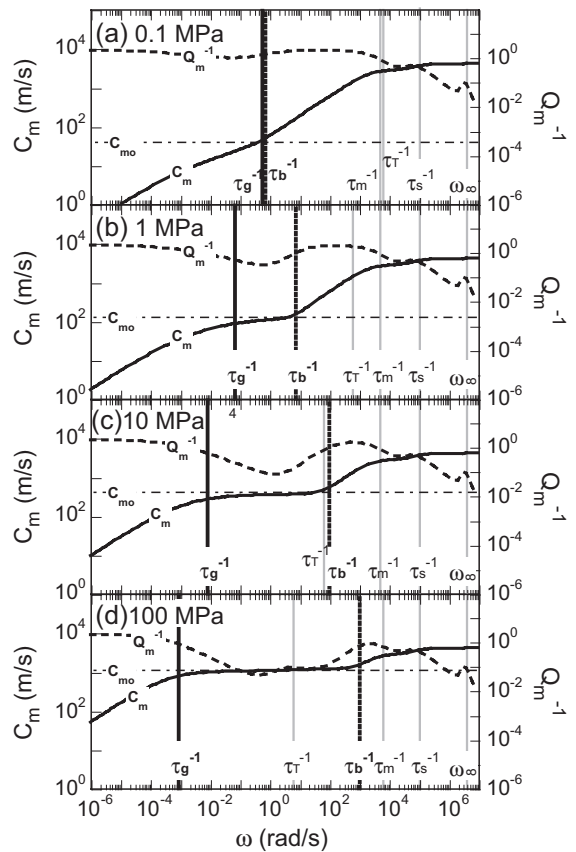

Fig. 7. The phase velocity (c_m) and the attenuation (Q_m^{-1}) of the pressure waves in the liquid–bubble mixture at various hydrostatic pressures (P_o). The magma viscosity (η_o) is assumed as 10^5 Pa s. The other parameters are the same as in Fig. 6. The characteristic frequencies of the acoustic properties of the mixture (Table 2) are indicated with the lines. The horizontal dash-and-dot line represents the value of c_{mo} defined by Eq. (39).

pressure wave in the mixture, respectively (Gaunaurd and Überall, 1981; Aki and Richards, 1980).

The frequency dependence of c_m and Q_m^{-1} are investigated for the conditions of the magmatic systems and presented in Figs. 6 and 7. The pressure is fixed at 1 MPa, and the viscosity of the magma is varied in Fig. 6, while the viscosity is fixed at 10^5 Pa s and the pressure is varied in Fig. 7. The other parameters are assumed as $\kappa_{gl} = 10^{-9}$ m^2/s for the volatile diffusivity in the liquid, $\phi = 0.03$

Table 2
The characteristic frequencies (rads) of the liquid–bubble mixture

Internal process	Symbol	Equation	α	P_o [MPa]			
				0.1	1	10	100
Heat transfer	τ_T^{-1}	(29)	R^{-2}	5.9×10^3	5.9×10^2	59	5.9
Mass transfer	τ_g^{-1}	(35)	R^{-2}	0.6	6.9×10^{-2}	8.0×10^{-3}	9.1×10^{-4}
Mixture volume relaxation	τ_m^{-1}	(21)	η_o^{-1}	4.5×10^8	4.5×10^8	4.6×10^8	5.4×10^8
Bubble volume relaxation	τ_b^{-1}	(40)	η_o^{-1}	9.8×10^4	9.8×10^5	9.8×10^6	9.8×10^7
Relaxed bubble resonance	ω_o	(17)	R^{-1}	1.2×10^4	3.9×10^4	1.2×10^5	3.9×10^5
Unrelaxed bubble resonance	ω_∞	(18)	R^{-1}	3.9×10^6	3.9×10^6	3.9×10^6	3.9×10^6

It is assumed that the temperature is 1273 K, the magma viscosity is 1 Pa s, the bubble radius is 1 mm and the void fraction is 0.03.

velocity and the attenuation factor on the frequency. The horizontal dash-and-dot line represents the value of c_{mo}:

$$c_{mo} = \sqrt{K_{mo}/\rho_m}, \tag{39}$$

where K_{mo} is defined in (22). Eq. (39) is frequently used to represent the sound speed in the liquid–bubble mixtures (e.g. Kiefer, 1977). However, the present results demonstrate that the phase velocity agrees with c_{mo} in the limited range of frequency.

When the viscosity is small and the bubble resonance occurs in the relaxed state of the liquid, the upper limit of the frequency range is determined by the resonance frequency of the bubble (Fig. 6a), as is expected from the analysis for the effective bulk modulus presented in Fig. 4. In the cases of the larger viscosities (Fig. 6b–d), the phase velocity gets larger than c_{mo} in the frequency range of $\omega > \tau_b^{-1}$ ($\tau_b^{-1} \ll \tau_m^{-1}$) in contrast with that the effective bulk modulus changes at $\omega \sim \tau_m^{-1}$ (Fig. 5). In fact, τ_b^{-1} is more important in the volcanology because ω_o is usually much higher than the frequency range of the observed volcanic phenomena (cf. Table 2). The expression for τ_b^{-1} is given below.

Analyzing Eq. (13), and considering the associated internal process of the volumetric motion of the bubbles, we found that τ_b^{-1} is simply estimated by:

$$\tau_b^{-1} = \frac{3K_g}{4\eta_o}. \tag{40}$$

Eq. (40) is obtained from the equation describing the viscosity-controlled radial motion of a bubble in an infinite Newtonian liquid:

$$4\eta_o \frac{\dot{R}}{R} = P_g - P_1, \tag{41}$$

where P_1 is the pressure in the liquid far from the bubble (Proussevitch et al., 1993). Assuming a small change of the bubble radius (δR) and using Eq. (1), Eq. (41) is linearized as:

$$4\eta_o \delta\dot{R} + 3K_g \delta R = -\delta P_1 R. \tag{42}$$

We can see that the characteristic solution is $\delta R = \exp(-t/\tau_b)$. The solution indicates that τ_b is the characteristic time of the viscous deformation of the bubble radius. If the time scale of the external pressure change is much longer than τ_b, change of the bubble radius can follow so that the mechanical equilibrium is maintained.

It is emphasized that the phase velocity and the attenuation of the pressure waves in the liquid–bubble mixture significantly depend on the frequency due to the several internal processes such as bubble expansion (contraction) and the volatile transfer. The sound speed of the liquid–bubble mixture is represented by c_{mo} only in the limited frequency range. The range is mainly bounded by τ_g^{-1} and τ_b^{-1}. Namely, c_{mo} is valid when the frequency of the pressure wave is large enough to keep the effect of the mass diffusion insignificant and small enough for the bubble radius to follow the pressure change.

5. Discussion

5.1. Implications to resonance behaviors of a magma body

Let us suppose a bubbly layer in a semi-infinite body of magma (Fig. 8). A plane pressure wave generated deep in the magma propagates through the layer and is transmitted to the air. We demonstrate the influence of the wave dispersion and attenuation of the bubbly layer on the response of the system by solving the simple one-dimensional problem. The positions of the top and the bottom of the bubbly layer are denoted by z_t and z_b, respectively, and the position of the magma surface is denoted by $z_0 = 0$. The hydrostatic pressure of the layer is approximated by $P_o = P_{air} + \rho_l g z_t$, where P_{air} is the atmospheric pressure (10^5 Pa) and g is the gravitational acceleration. The hydrostatic gradient within the layer is neglected for simplicity. Although the model is rather artificial, the main purpose here is to demonstrate the basic features of the effect of the wave dispersion.
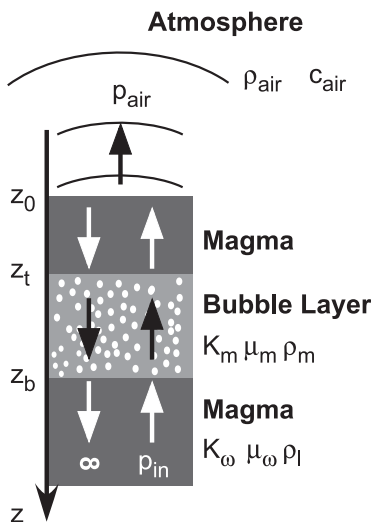
Atmosphere

Fig. 8. A simple example system to demonstrate how the resonance behavior of a body of bubbly magma is influenced by its frequency-dependent acoustic properties. A layer of bubbly region is assumed in the magma. A plane P-wave penetrates into the layer from below. It is partly reflected at the boundaries, but partly transmitted into the atmosphere. The frequency dependence of the wave transmission is calculated.

We apply the mathematical method presented by Kennet and Kerry (1979) to calculate the effective transmission coefficient of the layered medium. The method is described in a companion paper (Marchetti et al., 2004), so that only the equations used in the calculation are presented in Appendix B. The ratio of the pressure wave transmitted to the air (p_{air}) to the incident wave (p_{in}) is calculated by:

$$\left| \frac{p_{air}}{p_{in}} \right| = \left| T_U(z_0^-, z_b^+) \frac{p_{air} c_{air}}{K_\omega} \sqrt{\frac{K_\omega + \frac{4}{3}\mu_\omega}{\rho_l}} \right|, \qquad (43)$$

where ρ_{air} and c_{air} are the density and the sound speed of the atmosphere, respectively, and $T_U(z_0^-, z_b^+)$, which is given by (B1), is the effective transmission coefficient from beneath the bubbly layer (z_b^+) to just above the magma surface (z_0^-). Assuming that the temperature of the air at z_0^- is the same as that of the magma (1273 K), $\rho_{air} = 0.27$ kg/m^3 and $c_{air} = 720$ m/s.

We take the magma viscosity (η_o) and the bubble radius (R) as variable parameters in the following analyses. The hydrostatic pressure in the bubbly layer is fixed at $P_o = 1$ MPa, which corresponds to the depth of the layer of $z_t = 35.3$ m. The void fraction is assumed as $\phi = 0.03$. Eq. (39) gives $c_{mo} = 114$ m/s at this condition. The thickness of the bubbly layer is assumed as the half-wave length of a 1-Hz wave with this speed. Namely, $z_b - z_t = c_{mo}/2 = 57$ m.

The response of the system (Eq. (43)) is presented as a function of frequency in Figs. 9 and 10. In Fig. 9, the bubble radius is fixed at $R = 10^{-3}$ m and the viscosity is varied, while the viscosity is fixed at $\eta_o = 10^4$ Pa s and the bubble radius is changed in Fig. 10. The solid and broken vertical lines in the figures present τ_g^{-1} and τ_b^{-1}, respectively, defining the frequency range in which the sound speed c_{mo} is valid. These characteristic frequencies change with the viscosity and the bubble radius as $\tau_b^{-1} \propto \eta_o^{-1}$ and $\tau_g^{-1} \propto R^{-2}$ (Table 2).

The peaks of the response curves in Figs. 9 and 10 indicate the resonant frequencies of the layered medium. The resonance occurs due to the existence of the impedance contrast between the bubbly layer and the bubble-free layers. We can see that those peaks appear on condition that they are included in the range of
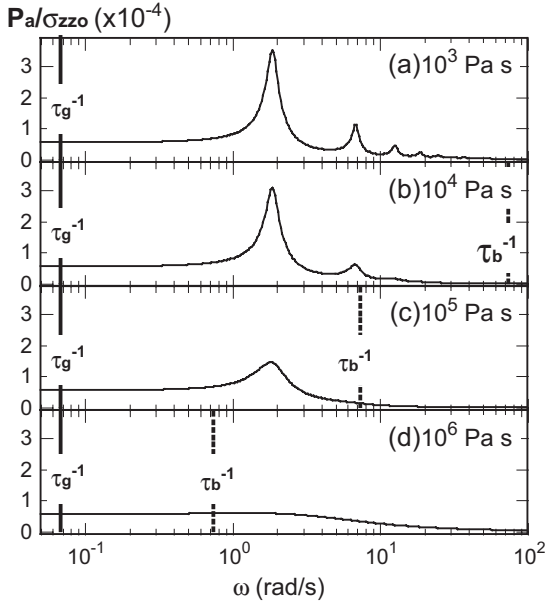
Fig. 9. The frequency dependence of the wave transmission from the magma to the air through the bubbly layer as shown in Fig. 8. The depth of the layer is fixed at $z_t = 35.3$ m ($P_o = 1$ MPa). The layer thickness is assumed as $z_b - z_t = 57$ m. The magma viscosity (η_o) is varied as (a) 1 Pa s, (b) 10^3 Pa s, (c) 10^6 Pa s and (d) 10^9 Pa s. The other parameters are the same as in Fig. 6. The dispersion relations for the conditions corresponding to (a) and (d) are presented in Fig. 6b and c, respectively.

$\tau_g^{-1} < \omega < \tau_b^{-1}$. The resonance fails outside the range because the attenuation is too large ($\omega \lesssim \tau_g^{-1}$, $\omega \sim \tau_b^{-1}$) or the impedance contrast is too weak ($\omega \gg \tau_b^{-1}$).

5.2. Applicability to the actual volcanic systems

The present expression for the effective properties of the liquid–bubble mixture includes the effects of the viscoelasticity of the liquid and the heat and mass transfer between the liquid and bubbles. The actual magmatic systems contain many other processes. Here, we discuss the effects of possible important factors.

5.2.1. Interaction between the bubbles

If we are to include the effect of the interaction between bubbles in the present mathematical framework to calculate the effective acoustic properties of a liquid–bubble mixture, we have to consider the

multiple scattering. This effect has been treated by Varadan et al. (1985) in calculating the phase velocity and attenuation of the pressure wave in the liquid–bubble mixture without the effect of viscosity. Their results agree with the other simpler calculations neglecting multiple scattering for the mixture with a small void fraction. The existing experimental results have also been explained by the simpler theories quite well (Commander and Prosperetti, 1989; Prosperetti, 1984; Gaunaurd and Überall, 1981; Ichihara et al., 2004). The maximum void fraction to which the single-scattering theories are applicable is generally regarded as several percents (Toksöz and Cheng, 1980). Unfortunately, there are few experimental data with which we can check their applicability to the higher void fractions. Not on the wave propagation, but Llewellin et al. (2002) presented experimental data on shear viscosity of liquid–bubble mixture with void fractions up to 46.1%. Their data demonstrated the linear relations between the void fraction and the effective shear viscosity of
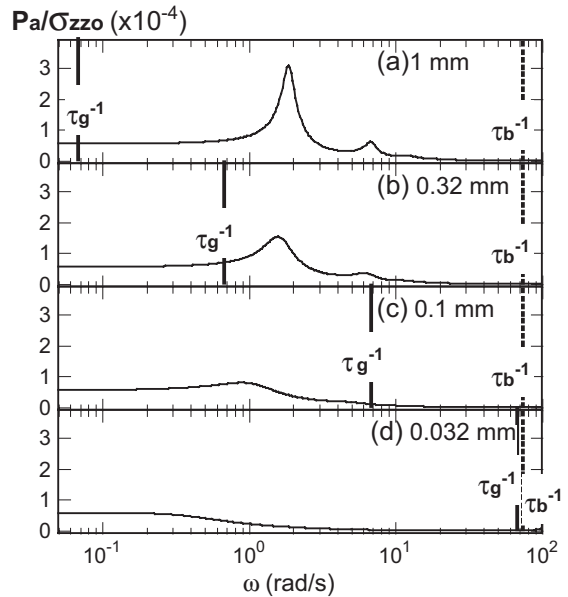

Fig. 10. The frequency dependence of the wave transmission from the magma to the air through the bubbly layer as shown in Fig. 8. The depth of the layer is fixed at $z_t = 35.3$ m ($P_o = 1$ MPa). The layer thickness is assumed as $z_b - z_t = 57$ m. The magma viscosity (η_o) is fixed at 10^4 Pa s, while the bubble radius is varied as (a) 1 mm, (b) 0.32 mm, (c) 0.1 mm and (d) 0.032 mm. The other parameters are the same as in Fig. 6.

the mixture: $\eta_m = \eta_o(1 - (5/3)\phi)$ for deformable bubbles, and $\eta_m = \eta_o(1 + 9\phi)$ for non-deformable bubbles. As is noted in Section 2.3, similar relations are derived from the present expression. This fact may partly support the applicability of the single scattering method to the higher void fractions.

5.2.2. Translational motion of the bubbles

The volatile transfer between the liquid and a bubble is affected by the flow around the bubble due to the translational motion of a bubble. We regard such an effect is unimportant, when the length scale of the bubble translation is much smaller than both the bubble radius and the diffusion layer thickness.

The terminal velocity of a spherical bubble under gravity is $u_b = A_t R^2 g \rho_l / \eta_o$, where $A_t = 1/3$ for a pure liquid and $2/9$ for a liquid with surfactants. The distance of the translational motion of a bubble in a time scale of the volatile diffusion is represented by:

$$u_b \tau_g = \frac{A_t g \rho_l}{9} \frac{R^4}{\eta_o \kappa_{gl} A_g^2}, \tag{44}$$

where the constant $A_t\, g\rho_l/9$ is about 630 and 950 for the pure and impure liquid, respectively. On the other hand, the thickness of the diffusion layer at $\omega = \tau_g^{-1}$ is:

$$\sqrt{\kappa_{gl}\tau_g} = R/(3A_g). \tag{45}$$

The condition required to neglect the effect of the translational motion is:

$$u_b\tau_g \ll R, \tag{46}$$

$$u_b\tau_g \ll \sqrt{\kappa_{gl}\tau_g}. \tag{47}$$

The conditions (46) and (47) are rewritten as:

$$\eta_o \gg \frac{A_t g \rho_l}{9} \frac{R^3}{\kappa_{gl} A_g^2}, \tag{48}$$

$$\eta_o \gg \frac{A_t g \rho_l}{3} \frac{R^3}{\kappa_{gl} A_g}, \tag{49}$$

respectively. The condition (48) is defining for $A_g < 1/3$, while condition (49) is defining for $A_g > 1/3$. The condition is presented on the $R-\eta_o$ plane in Fig. 11 as the region above the line for each pressure.

5.2.3. Existence of highly deformed or connected bubbles

We have presented that the sound speed is not efficiently decreased by the presence of bubbles in a high-viscosity magma assuming the spherical bubbles. On the other hand, it has been shown for porous solids that a small amount of thin pores can significantly decrease the elastic moduli and seismic velocities, which are rather insensitive to the rounder or spherical pores (Toksöz et al., 1976). It is because the thinner pores are more deformable due to the stress concentration along the arc with the highest curvature. Furthermore, in a system consisting of connected bubbles, another kind of slow wave controlled by the permeable gas flow exists (Biot, 1956; Shoenberg, 1983). It is certain that these matters are involved in the volcanic systems and should be studied in more detail. However, observations of natural porous volcanic rocks have shown that the amount of interconnected irregular network of bubbles is drastically reduced below a void fraction of 50% (Spieler et al., 2004). Therefore, we consider that, in the actual volcanic processes, there are a number of situations where the present formulation and analyses are useful.
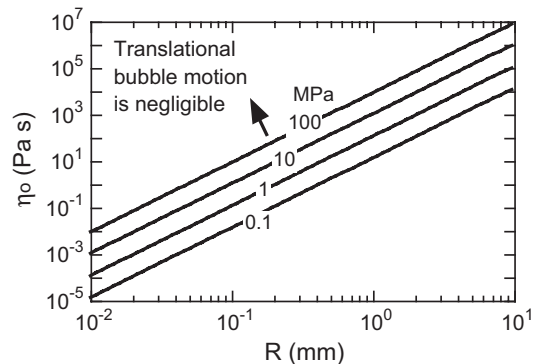

Fig. 11. The minimum viscosity that makes the translational motion of a bubble negligible as a function of the bubble radius and the pressure.

5.2.4. Inhomogeneous bubble distribution and the hydrostatic pressure gradient

The actual magma column is supposed to be spatially inhomogeneous. The hydrostatic pressure gradient and the resultant variation of the void fraction cannot be ignored. Wave propagation in such a vertically inhomogeneous two-phase system is treated in the companion paper (Marchetti et al., 2004).

6. Summary

(1)   The effective acoustic properties of a liquid–bubble mixture are represented by Eqs. (13)–(16) with Eq. (4) representing the effective bulk modulus of a bubble. These equations include effects of the bubble resonance, the heat and the mass transfer between the liquid and bubbles, and the viscoelasticity of the liquid. Using these equations, the phase velocity and attenuation factor of the pressure wave in the mixture are calculated by Eqs. (36)–(38) as functions of the frequency.

(2)   We defined seven characteristic times and frequencies associated with the internal processes controlling the dispersion and attenuation of the pressure waves in the bubbly magmas: the relaxation time of the melt (τ_s: Eq. (9)), that of the volumetric deformation of the mixture (τ_m: Eq. (21)), the characteristic time of the viscosity-controlled bubble expansion (contraction) (τ_b: Eq. (40)), that of the heat transfer in the bubble (τ_T:Eq. (29)), that of the volatile transfer (τ_g: Eq. (35)), and the resonance frequency of the bubble in the relaxed or the unrelaxed condition (ω_o: Eq. (17) or ω_∞: Eq. (18)). They are all represented by simple functions of the material and condition parameters.

(3)   The phase velocity of the pressure wave agrees with c_{mo} (Eq. (39)) only in the limited range of the frequency, though it is often used to represent the sound speed of the liquid–bubble mixture. In most of the cases with the magmatic systems, τ_g^{-1} and τ_b^{-1} determine the lower and upper limits of the frequency range.

(4)   Resonance behavior of a bubbly layer of magma is caused by the impedance contrast between the layer and the surrounding medium. It is noted that such resonance can occur on condition that the resonance frequencies are within the range bounded by τ_g^{-1} and τ_b^{-1}.

The present study demonstrated that the frequency dependence of the phase velocity and attenuation of the pressure waves is considerable in the bubbly magma. However, it is not always easy to include such effects in the existing mathematical framework to calculate the wave field in the elastic medium. Therefore, we propose the following simple way to use the present result in constructing a model for the seismo-acoustic phenomena of volcanoes:

(1)   Assume that the bubbly magma is an elastic medium with the slow sound speed, c_{mo}, and calculate the wave field.

(2)   Calculate the characteristic frequencies for volatile diffusion (τ_g^{-1}) and bubble expansion (τ_b^{-1}) in the system.

(3)   Make sure that the natural phenomenon to which the model is applied is in the frequency range of $\tau_g^{-1} < \omega < \tau_b^{-1}$, where the sound speed of c_{mo} is applicable.

Appendix A. Derivation of the equations to calculate the effective bulk modulus of a bubble

A.1. Equations for pressure and temperature in the bubble

When the bubble radius changes periodically, diffusion layers of temperature and volatile concentration are formed around the bubble. It is assumed that distances between the bubbles are much larger than the thickness of the layers and we consider a single bubble in an infinite body of a liquid.

A mass conservation equation for the gas is:

$$\frac{\partial \rho_g}{\partial t} + \frac{1}{r^2} \frac{\partial}{\partial r}(r^2 \rho_g u_g) = 0, \tag{A1}$$

where r is the distance from the center of the bubble, ρ_g is the density, and u_g is the radial velocity of the gas.

We assume that the gas in a bubble is an ideal gas:

$$P_g = \rho_g R_g T, \tag{A2}$$

where R_g is the gas constant, and T is the temperature.

Energy conservation of the gas in a bubble is represented as:

$$\frac{d}{dt}\left(\frac{P_g}{\gamma - 1}\right) + \frac{1}{r^2} \frac{\partial}{\partial r}\left(r^2 \frac{P_g u_g}{\gamma - 1}\right)$$
$$= -\frac{1}{r^2} \frac{\partial}{\partial r}[r^2 P_g u_g] + \lambda_g \frac{1}{r^2} \frac{\partial}{\partial r}\left(r^2 \frac{\partial T}{\partial r}\right), \tag{A3}$$

where λ_g is the heat conductivity of the gas.

Considering a wave field in which the wavelength is much larger than the size of the bubbles, it is assumed that P_g is uniform in the bubble. Then Eq. (A3) is integrated from $r = 0$ to r as:

$$u_g = \frac{1}{\gamma P_g}\left[(\gamma - 1)\lambda_g \frac{\partial T}{\partial r} - \frac{r}{3}\dot{P}_g\right], \tag{A4}$$

where the superimposed dot indicates d/dt. Substituting Eqs. (A2) and (A4) into Eq. (A1), a differential equation for the temperature is obtained:

$$\frac{\partial T}{\partial t} + u_g \frac{\partial T}{\partial r} = \kappa_T \frac{1}{r^2} \frac{\partial}{\partial r}\left(r^2 \frac{\partial T}{\partial r}\right) + \frac{\gamma - 1}{\gamma} \frac{T}{P_g}\dot{P}_g, \tag{A5}$$

$$\kappa_T = \frac{\lambda_g}{\rho_g} \frac{\gamma - 1}{\gamma R_g}, \tag{A6}$$

where κ_T is the thermal diffusivity of the gas and $\gamma R_g/(\gamma - 1)$ is the heat capacity of an ideal gas at a constant pressure.

Mass flux of the volatile through the bubble wall ($\dot{M}_g$) is defined as:

$$\rho_g(u_g - \dot{R}) = -\dot{M}_g, \tag{A7}$$

where R is the bubble radius. Substituting Eq. (A7) into Eq. (A4) at $r = R$, a differential equation for the pressure is obtained as:

$$\dot{P}_g = \frac{3(\gamma - 1)}{R}$$
$$\times \left[\lambda_g \left(\frac{\partial T}{\partial t}\right)_w - \frac{\gamma}{\gamma - 1}P_g\dot{R} + \frac{\gamma}{\gamma - 1}TR_g\dot{M}_g\right], \tag{A8}$$

where the subscript w indicate the value at $r = R$.

A.2. Equations for heat and mass transfer in the liquid and at the bubble wall

The temperature of the liquid is assumed to be constant (T_o), because the heat conductivity and the heat capacity of liquid are much larger than those of the gas. Moreover, the latent heat associate with the volatile transfer between the gas and liquid phases is neglected. Then the boundary condition for the temperature at the bubble wall ($r = R$) is:

$$T_w = T_o. \tag{A9}$$

Transfer of the volatile in the liquid is described by:

$$\frac{\partial C_g}{\partial t} + u_l \frac{\partial C_g}{\partial r} = \kappa_{gl} \frac{1}{r^2} \frac{\partial}{\partial r}\left(r^2 \frac{\partial C_g}{\partial r}\right), \tag{A10}$$

where u_l is the radial velocity, and C_g and κ_{gl} are the concentration and the diffusivity of the volatile in liquid. The mass flux of the volatile at the bubble wall is:

$$\dot{M}_g = \rho_l \kappa_{gl}\left(\frac{\partial C_g}{\partial r}\right)_w. \tag{A11}$$

We assume that gas concentration at the interface is in equilibrium with the gas phase and determined by the pressure in the bubble according to the Henry's law:

$$C_{gw} = C_{eq}(P_g). \tag{A12}$$

A.3. Linear analysis

We define dimensionless variables, which are denoted with asterisks:

$$
\left.
\begin{aligned}
t &= \omega^{-1} t_*, & r &= R_o r_*, \\
R &= R_o(1 + R_*), & P_g &= P_o(1 + P_*), \\
T &= T_o(1 + T_*), & C_g &= C_{go}(1 + C_*),
\end{aligned}
\right\} \tag{A13}
$$

where the center of the oscillation for each variable is denoted with subscript o, and ω is the angular frequency of the oscillation. The following dimensionless parameters are defined:

$$\Theta^2 = \frac{2R_o^2 \omega}{\kappa_T}, \tag{A14}$$

$$\alpha_g = \frac{\kappa_{gl}}{\kappa_T} \tag{A15}$$

$$X_g = \frac{\rho_l C_{go}}{\rho_{go}}, \tag{A16}$$

$$H_n = \frac{P_o}{C_{go}} \frac{\partial C_{eq}}{\partial P}. \tag{A17}$$

The dimensionless variables (Eq. (A13)) are substituted into Eqs. (A8), (A5) and (A10) and the equations are linearized with respect to the perturbations. Using relations (A2), (A6), (A11) and (A14)–(A17), we obtain:

$$\dot{P}_* = \frac{6\gamma}{\Theta^2}\left[\left(\frac{\partial T_*}{\partial r_*}\right)_w - \frac{\Theta^2 \dot{R}_*}{2} + X_g \alpha_g \left(\frac{\partial C_{1*}}{\partial r_*}\right)_w\right], \tag{A18}$$

$$\frac{\partial T_*}{\partial t_*} = \frac{2}{\Theta^2}\frac{1}{r_*^2}\frac{\partial}{\partial r_*}\left(r_*^2 \frac{\partial T_*}{\partial r_*}\right) + \frac{\gamma - 1}{\gamma}\dot{P}_*, \tag{A19}$$

$$\frac{\partial C_*}{\partial t_*} = \frac{2\alpha_g}{\Theta^2}\frac{1}{r_*^2}\frac{\partial}{\partial r_*}\left(r_*^2 \frac{\partial C_*}{\partial r_*}\right). \tag{A20}$$

The dimensionless boundary conditions at $r_* = 1$ are:

$$T_* = 0, \tag{A21}$$

$$C_* = H_n P_*. \tag{A22}$$

We consider a periodic system in which all the variables are proportional to e^{-it_*}. The pressure and the bubble radius, which are independent of r_*, are:

$$P_* = e^{-it_*}\tilde{P}, \tag{A23}$$

$$R_* = e^{-it_*}\tilde{R}. \tag{A24}$$

Equations are solved with the constraint that the perturbation variables are finite at the center of the bubble ($r_* = 0$), and vanishes far from the bubble ($r_* = \infty$):

$$T_* = e^{-it_*}\tilde{P}\left[\tilde{T}\frac{\sinh\left(r_*\Theta\sqrt{\frac{-i}{2}}\right)}{r_*\sinh\left(\Theta\sqrt{\frac{-i}{2}}\right)} + \frac{\gamma - 1}{\gamma}\right], \tag{A25}$$

$$C_* = e^{-it_*}\tilde{P}\tilde{C}\frac{\exp\left(-r_*\Theta\sqrt{\frac{-i}{2\alpha_g}}\right)}{r_*\exp\left(-\Theta\sqrt{\frac{-i}{2\alpha_g}}\right)}. \tag{A26}$$

Here, note that $\sqrt{-i/2} = (1 - i)/2$.

The coefficients $\tilde{T}$ and $\tilde{C}$ are determined from the boundary conditions (A21) and (A22) as:

$$\tilde{T} = -\frac{\gamma - 1}{\gamma}, \tag{A27}$$

$$\tilde{C} = H_n. \tag{A28}$$

Substituting solutions (A23)–(A26) into Eq. (A18), we obtain:

$$\tilde{P} = -3F(\Theta)\tilde{R}, \tag{A29}$$

$$F(\Theta) = \frac{-i}{2}\gamma\Theta^2 / \left\{ \frac{-i}{2}\Theta^2 + 3(\gamma - 1)\left[-1 + \right. \right.$$

$$\left. \Theta\sqrt{\frac{-i}{2}}\tanh^{-1}\left(\Theta\sqrt{\frac{-i}{2}}\right)\right]$$

$$q3pt + 3\gamma X_g H_n\left(\alpha_g + \Theta\sqrt{\frac{-i\alpha_g}{2}}\right)\right\}. \tag{A30}$$

Comparing Eqs. (A18) and (1), $F(\Theta)$ is regarded as the dimensionless bulk modulus of the bubble:

$$\frac{K_g}{P_o} = F(\Theta). \tag{A31}$$

Eq. (4) is obtained by transformation of Eq. (A30).

Appendix B. The effective transmission coefficient of the layers

We consider a wave field depending on time through $e^{-i\omega t}$. According to Appendix A in Marchetti et al. (2004), the transmission coefficient of the layered medium (Fig. 8) is expressed as follows. The terms $K_\alpha + (4/3)\mu_\alpha$ ($\alpha = \omega, m$) in the following equations correspond to $\rho c^2 + i\omega(4/3)\eta_{\text{eff}}$ in the other paper. It is noted that the wave field is assumed as $\propto e^{i\omega t}$ in the other paper. Namely, all the expressions are complex conjugate with each other in the two papers:

$$T_U(z_0^-, z_b^+) = q_{11} - q_{12}q_{22}^{-1}q_{21} \tag{B1}$$

$$\begin{pmatrix} q_{11} & q_{12} \\ q_{21} & q_{22} \end{pmatrix} = \mathbf{D}^{-1}(z_0^-)\mathbf{D}(z_0^+)\mathbf{E}(z_0^+, z_t^-)\mathbf{D}^{-1}(z_t^-)$$

$$\times \mathbf{D}(z_t^+)\mathbf{E}(z_t^+, z_b^-)\mathbf{D}^{-1}(z_b^-)\mathbf{D}(z_b^+)$$

$$\mathbf{D}(z_0^-) = \begin{pmatrix} 1 & 1 \\ -i\rho_{air}c_{air} & i\rho_{air}c_{\text{air}} \end{pmatrix}$$

$$\mathbf{D}(z_0^+) = \mathbf{D}(z_t^-) = \mathbf{D}(z_b^+)$$

$$= \begin{pmatrix} 1 & 1 \\ -i\sqrt{\rho_l\left(K_\omega + \frac{4}{3}\mu_\omega\right)} & i\sqrt{\rho_l\left(K_\omega + \frac{4}{3}\mu_\omega\right)} \end{pmatrix}$$

$$\mathbf{D}(z_t^+) = \mathbf{D}(z_b^-)$$

$$= \begin{pmatrix} 1 & 1 \\ -i\sqrt{\rho_m\left(K_m + \frac{4}{3}\mu_m\right)} & i\sqrt{\rho_m\left(K_m + \frac{4}{3}\mu_m\right)} \end{pmatrix}$$

$$\mathbf{E}(z_0^+, z_t^-) = \begin{pmatrix} e^{-ik_\omega(z_0^+ - z_t^-)} & 0 \\ 0 & e^{ik_\omega(z_0^+ - z_t^-)} \end{pmatrix}$$

$$\mathbf{E}(z_t^+, z_b^-) = \begin{pmatrix} e^{-ik_\omega(z_t^+ - z_b^-)} & 0 \\ 0 & e^{ik_\omega(z_t^+ - z_b^-)} \end{pmatrix}$$

where the complex wave number in the magma is given by $k\omega = \omega\sqrt{\rho_l/(K_\omega + \frac{4}{3}\mu_\omega)}$ with K_ω and μ_ω given in Eqs. (7) and (8), respectively, and k_m is given in Eq. (36).

References

Aki, K., Richards, P., 1980. Quantitative Seismology. Freeman, New York.

Benoit, J.P., McNutt, S.R., 1997. New constraints on source processes of volcanic tremor at Arenal volcano, Costa Rica, using broadband seismic data. Geophys. Res. Lett. 24, 449–452.

Biot, M.A., 1956. Theory of propagation of elastic waves in a fluid-saturated porous solid: I. Low frequency range. J. Acoust. Soc. Am. 28, 168–178.

Bowers, T.S., 1995. Pressure–volume–temperature properties of H2O CO2 fluids. In: Ahrens, T.J. (Ed.), (Ed.), A Handbook of Physical Constants: Rock Physics and Phase Relations. AGU Reference Shelf Series, vol. 3. AGU, pp. 45–72.

Caflish, R.E., Miksis, M.J., Papanicolaou, G.C., Ting, L., 1985. Ef-

fective equation for wave propagation in bubbly liquids. J. Fluid Mech. 153, 259–273.

Cheyne, S.A., Stebbings, C.T., Roy, R.A., 1995. Phase velocity measurements in bubbly liquids using a fiber optic laser interferometer. J. Acoust. Soc. Am. 97, 1621–1624.

Chouet, B.A., 1996. New methods and future trends in seismological volcano monitoring. In: Scarpa, R., Tilling, R.I. (Eds.), (Eds.), Monitoring and Mitigation of Volcano Hazards. Springer-Verlag, Berlin, pp. 23–97.

Commander, K.W., Prosperetti, A., 1989. Linear pressure waves in bubbly liquids: comparison between theory and experiments. J. Acoust. Soc. Am. 85, 732–746.

Dingwell, D.B., 1998. Recent experimental progress in the physical description of silicic magma relevant to explosive volcanism. In: Gilbert, J.S., Sparks, R.S.J. (Eds.), (Eds.), The Physics of Explosive Volcanic Eruptions. Geol. Soc. London, pp. 9–26.

Dingwell, D.B., Webb, S.L., 1989. Structural relaxation in silicate melts and non-Newtonian melt rheology in geologic processes. Phys. Chem. Miner. 16, 508–516.

Garces, M.A., 1997. On the volcanic waveguide. J. Geophys. Res. 102, 22547–22564.

Garces, M.A., McNutt, S.R., 1997. Theory of the sound field generated by a resonant magma conduit. J. Volcanol. Geotherm. Res. 78, 155–178.

Gaunaurd, G.C., Überall, H., 1981. Resonance theory of bubbly liquids. J. Acoust. Soc. Am. 69, 362–370.

Holloway, J.R., Blank, J.G., 1994. Application of experimental results to C–O–H species in natural melts. In: Carroll, M.R., Holloway, J.R. (Eds.), (Eds.), Volatiles in Magmas. Rev. Miner., 30, 187–230.

Ichihara, M., Ohkunitani, H., Ida, Y., Kameda, M., 2004. Dynamics of bubble oscillation and wave propagation in viscoelastic liquids. J. Volcanol. Geotherm. Res. 129, 37–60.

JSME, 1983. Thermodynamic properties of fluids, JSME technical reference series. J. Jpn. Soc. Mech. Eng., 547.

Kennet, L.N., Kerry, N.J., 1979. Seismic waves in a stratified half space. Geophys. J. R. Astron. Soc. 57, 557–583.

Khitarov, N.I., Lebedev, E.B., Dorfman, A.M., Bagdasarov, N.S., 1979. Effect of temperature, pressure and volatile components upon the surface-tension of basaltic melt. Geokhimiya 10, 1427–1438.

Kiefer, S.W., 1977. Sound speed in liquid–gas mixtures: water–air and water–steam. J. Geophys. Res. 82, 2895–2904.

Kumagai, H., Chouet, B., 2000. Acoustic properties of a crack containing magmatic or hydrothermal fluids. J. Geophys. Res. 105, 25493–25512.

Kuster, G.T., Toksöz, M.N., 1974. Velocity and attenuation of seismic waves in two-phase media: 1. Theoretical formulations. Geophysics 39, 587–606.

Lensky, N.G., Syakhovsky, V., Navon, O., 2002. Expansion dynamics of volatile-supersaturated liquids and bulk viscosity of bubbly magmas. J. Fluid Mech. 460, 39–56.

Llewellin, E.W., Mader, H.M., Wilson, S.D.R., 2002. The rheology of a bubbly liquid. Proc. R. Soc. London, A 458, 987–1016.

Mackenzie, J.K., 1950. Elastic constants of a solid containing spherical holes. Proc. Phys. Soc. Lond. B63, 2–11.

Marchetti, E., Ichihara, M., Ripepe, M., 2004. Propagation of acoustic waves in a visco-elastic two-phase system: influence of the gas bubble concentration. J. Volcanol. Geotherm. Res. 137, 93–108 (this issue).

Massol, H., Jaupart, C., 1999. The generation of gas overpressure in volcanic eruptions. Earth Planet. Sci. Lett. 166, 57–70.

Murase, T., McBirney, R., 1973. Properties of some common igneous rocks and their melt at high temperature. Geol. Soc. Amer. Bull. 84, 3563–3592.

Neuberg, J., Luckett, R., Baptie, B., Olsen, K., 2000. Models of tremor and low-frequency earthquake swarms on Montserrat. J. Volcanol. Geotherm. Res. 101, 83–104.

Nowak, M., Behrens, H., 1997. An experimental investigation on diffusion of water in haplogranitic melts. Contrib. Mineral. Petrol. 126, 365–376.

Prosperetti, A., 1984. Bubble phenomena in sound fields 2. Ultrasonics 22, 115–124.

Prosperetti, A., 1991. The thermal behavior of oscillating gas bubbles. J. Fluid Mech. 222, 587–616.

Proussevitch, A.A., Sahagian, D.L., Kutolin, V.A., 1993. Stability of foams in silicate melts. J. Volcanol. Geotherm. Res. 59, 161–178.

Shoenberg, M., 1983. Wave propagation in a finely laminated periodic elastoacoustic medium. Appl. Phys. Lett. 42, 350–352.

Sibree, J.O., 1934. The viscosity of froth. Trans. Faraday Soc. 28, 325–331.

Silberman, E., 1957. Sound velocity and attenuation in bubbly mixtures measured in standing wave tubes. J. Acoust. Soc. Am. 29, 925–933.

Sparks, R.S.J., Barklay, J., Jaupart, C., Mader, H.M., Phillips, J.C., 1994. Physical aspects of magmatic degassing I. Experimental and theoretical constraints on vesiculation. In: Carrol, M.R., Holloway, J.R. (Eds.), (Eds.), Volatiles in Magmas. Rev. Mineral., 30, 413–443.

Spieler, O., Dingwell, D.B., Alidibirov, M., 2004. Magma fragmentation speed: an experimental determination. J. Volcanol. Geotherm. Res. 129, 109–123.

Stein, D.J., Spera, F.J., 1992. Rheology and microstructure of magmatic emulsions: theory and experiments. J. Volcanol. Geotherm. Res. 49, 157–174.

Toksöz, M.N., Cheng, C.H., 1980. Velocities of seismic waves in composite, multi-phase media. J. Acoust. Soc. Am. Suppl. 1 (67), S43.

Toksöz, M.N., Cheng, C.H., Timur, A., 1976. Velocities of seismic-waves in porous rocks. Geophysics 41, 621–645.

Varadan, V.K., Varadan, V.V., Ma, Y., 1985. A propagator model for scattering of acoustic waves by bubbles in water. J. Acoust. Soc. Am. 78, 1879–1881.

Webb, S.L., 1997. Silicate melts: relaxation, rheology, and glass transition. Rev. Geophys. 35, 191–218.

Webb, S.L., Dingwell, D.B., 1995. Viscoelasticity. In: Stebbins, J.F., McMillan, P.F., Dingwell, D.B. (Eds.), (Eds.), Structure, Dynamics, and Properties of Silicate Melts. Rev. Mineral., 32, 95–119.

Zhang, Y.X., Behrens, H., 2000. H_2O diffusion in rhyolitic melts and glasses. Chem. Geol. 169, 243–262.

Zhang, Y.X., Stolper, E.M., Wasserburg, G.J., 1991. Diffusion of a multispecies component and its role in oxygen and water transport in silicates. Earth Planet. Sci. Lett. 103, 228–240.